Structural asymmetry in the magnesium channel CorA points to sequential allosteric regulation

Roland Pfoh[a,b], Angela Li[a], Nilmadhab Chakrabarti[c], Jian Payandeh[b,d,1], Régis Pomès[a,c], and Emil F. Pai[a,b,d,e,2]

Departments of [a]Biochemistry, [d]Medical Biophysics, and [e]Molecular Genetics, University of Toronto, Toronto, ON, Canada, M5G 1L7; [b]Ontario Cancer Institute/Princess Margaret Cancer Centre, Campbell Family Institute for Cancer Research, Toronto, ON, Canada, M5G 1L7; and [c]Program in Molecular Structure and Function, Hospital for Sick Children, Toronto, ON, Canada, M5G 1X8

Edited by David E. Clapham, Howard Hughes Medical Institute, Children's Hospital Boston, Boston, MA, and approved September 27, 2012 (received for review May 30, 2012)

Magnesium ions (Mg^{2+}) are essential for life, but the mechanisms regulating their transport into and out of cells remain poorly understood. The CorA-Mrs2-Alr1 superfamily of Mg^{2+} channels represents the most prevalent group of proteins enabling Mg^{2+} ions to cross membranes. *Thermotoga maritima* CorA (TmCorA) is the only member of this protein family whose complete 3D fold is known. Here, we report the crystal structure of a mutant in the presence and absence of divalent ions and compare it with previous divalent ion-bound TmCorA structures. With Mg^{2+} present, this structure shows binding of a hydrated Mg^{2+} ion to the periplasmic Gly-Met-Asn (GMN) motif, revealing clues of ion selectivity in this unique channel family. In the absence of Mg^{2+}, TmCorA displays an unexpected asymmetric conformation caused by radial and lateral tilts of protomers that leads to bending of the central, pore-lining helix. Molecular dynamics simulations support these movements, including a bell-like deflection. Mass spectrometric analysis confirms that major proteolytic cleavage occurs within a region that is selectively exposed by such a bell-like bending motion. Our results point to a sequential allosteric model of regulation, where intracellular Mg^{2+} binding locks TmCorA in a symmetric, transport-incompetent conformation and loss of intracellular Mg^{2+} causes an asymmetric, potentially influx-competent conformation of the channel.

crystallography | gating | limited proteolysis | pentamer

Compared with other common biological ions (Na^+, K^+, Ca^{2+}, Cl^-), very little is known on a molecular level about the cellular homeostasis of Mg^{2+}. As the most abundant intracellular divalent cation, it stabilizes phosphate compounds (DNA, RNA, ATP) and their synthesis, is essential for the function of over 300 enzymes, and is central to photosynthesis in plants (1). In addition to antagonizing Ca^{2+} signaling (2), Mg^{2+} has recently been implicated as a key second messenger in T-cell activation through the MagT1 Mg^{2+} channel (3). The CorA protein is the primary transport system for Mg^{2+} in Bacteria and Archaea and is required for bacterial pathogenesis (4, 5). It can functionally substitute for its eukaryotic homologs Alr1 and Mrs2 (6, 7), suggesting that CorA represents an important model system for these eukaryotic Mg^{2+} channels. Alr1 is the major Mg^{2+} uptake system in the plasma membrane of yeast (8), and Mrs2 is present in the inner mitochondrial membranes of yeast (6), plants (9), and mammals (10). Despite Mrs2 being essential for normal mitochondrial function (11), its expression is a hallmark of embryonic stem cells (12), and Mrs2 overexpression has been linked to a multidrug resistance phenotype in cancer (13, 14). Patch-clamp analysis established Mrs2 as a high-conductance (155 pS) Mg^{2+}-selective channel (15), and a similar conductivity has been indicated for CorA (16).

Three crystal structures of wild-type *Thermotoga maritima* CorA (TmCorA-WT), obtained in the presence of divalent cations (17–19), revealed a symmetric homopentamer with a large intracellular funnel linked to two transmembrane (TM) helices per monomer in an apparently closed state, establishing TmCorA as a structural template of the CorA-Mrs2-Alr1 superfamily (20). As seen in Fig. 1, the intracellular funnel domain is comprised of a core helical bundle consisting of α5, α6, and α7. Five ca. 100-Å-long α7 helices come together in a left-handed spiral (Fig. 2*A*), creating an ion pore unlike any other known channel. The C-terminal end of α7 spans the membrane (TM1), ending in the universally conserved Gly-Met-Asn (GMN) sequence. A short periplasmic loop connects it to α8 (TM2). Five α8 helices end in the cytosol, with the C-terminal KKKKWL motif in proximity to the α5-α6 loop of a neighboring monomer (Fig. 1*A*). Forming the outer wall of the funnel, α5 and α6 contain an unusual amount of negatively charged residues, which confront the basic sphincter (KKKKWL motif of α8 and K292 of α7). Two intracellular Mg^{2+}-binding sites (M1 and M2) function as an intracellular divalent cation sensor (DCS) between the intracellular end of α7 and α3′ (residues and distances in protomers B to E are indicated by the addition of prime symbols ′ to ′′′′), where M1 may be the primary regulatory site in TmCorA (21). In a recent computational study (22), removal of the ten regulatory ions from M1 and M2 led to changes in the tilt of α7, resulting in an iris-like dilation of the pore and subsequent hydration of the hydrophobic pore region between M302 and M291 (MM stretch), suggesting an allosteric mechanism coupling intracellular Mg^{2+} concentration to hydrophobic gating. It has been further suggested that the acidic electrostatic nature of α5 and α6 might be used to change the position of the basic sphincter, which surrounds the tightest pore constriction formed by M291 (17). The periplasmic pore entrance is poorly resolved in all available crystal structures. This region is thought to bind a hexahydrated magnesium ion $[Mg(H_2O)_6]^{2+}$ because CorA is inhibited by its geometric analog cobalt hexamine $[Co(NH_3)_6]^{3+}$ (23). NMR studies on an isolated TM domain (24) report weak and dynamic binding of hydrated Mg^{2+} and $[Co(NH_3)_6]^{3+}$ to the periplasmic α7-α8 loop. However, a direct role for the GMN motif in selecting for Mg^{2+} remains unproven despite its conservation at the mouth of the pore. The pentameric organization of CorA further confounds our understanding of ion selectivity because this architecture does not fit the expected octahedral coordination geometry of Mg^{2+} (25).

All previous crystal structures of TmCorA-WT were obtained in the presence of high concentrations of Mg^{2+} or Ca^{2+}. In our hands, TmCorA-WT has resisted all crystallization attempts in the absence of divalent ions. However, we identified a TmCorA

Author contributions: R. Pfoh, A.L., N.C., J.P., R. Pomès, and E.F.P. designed research; R. Pfoh, A.L., N.C., and J.P. performed research; R. Pfoh, A.L., N.C., J.P., R. Pomès, and E.F.P. analyzed data; and R. Pfoh, J.P., R. Pomès, and E.F.P. wrote the paper.

The authors declare no conflict of interest.

This article is a PNAS Direct Submission.

Data deposition: The atomic coordinates and structure factors have been deposited in the Protein Data Bank, www.pdb.org (PDB ID codes 4EEB and 4EED).

[1]Present address: Department of Structural Biology, Genentech Inc., South San Francisco, CA 94080.

[2]To whom correspondence should be addressed. E-mail: pai@hera.med.utoronto.ca.

This article contains supporting information online at www.pnas.org/lookup/suppl/doi:10.1073/pnas.1209018109/-/DCSupplemental.

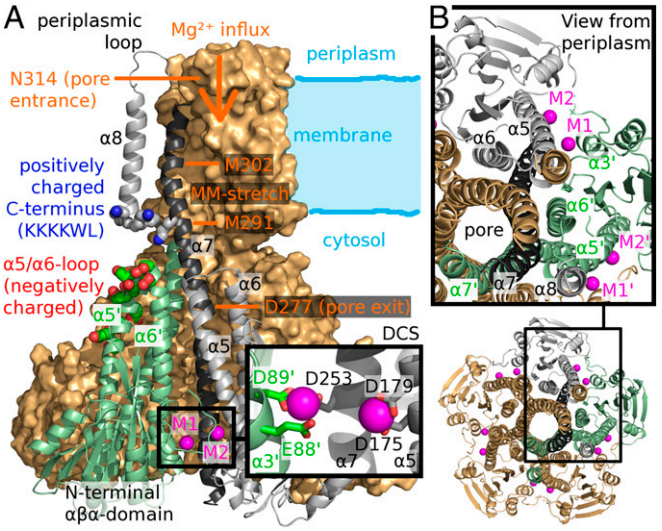

Fig. 1. CorA pentamer in the closed state. (*A*) Side view: cartoon representations of two adjacent protomers, protomer A (gray, full length) and B (green, cytosolic domain). Helix α7 of protomer A is colored dark gray, and adjacent α7 helices have been omitted for clarity. The three remaining protomers C/D/E are shown in surface representation (light orange). Mg^{2+} ions bound to the divalent cation sensor (DCS) are shown as magenta colored spheres. (*B*) Top-to-bottom view: The color code is the same as in *A*; protomers are shown full length in cartoon representation.

mutant that still responds to changes in Mg^{2+} concentration and can be crystallized both with and without divalent cations, trapping it in two different states. The first structure determined in the presence of Mg^{2+} (3.9-Å resolution) reveals two ions bound along the pore, with one coordinated at the GMN motif. Remarkably, the second structure determined in the absence of divalent ions (3.8-Å resolution) reveals a distinctly asymmetric architecture, which provides insight into an unexpected potential regulatory mechanism operating in this ubiquitous channel family. We complement our crystallographic studies with a time-extended (700 ns) molecular dynamics (MD) simulation and supporting biochemical assays.

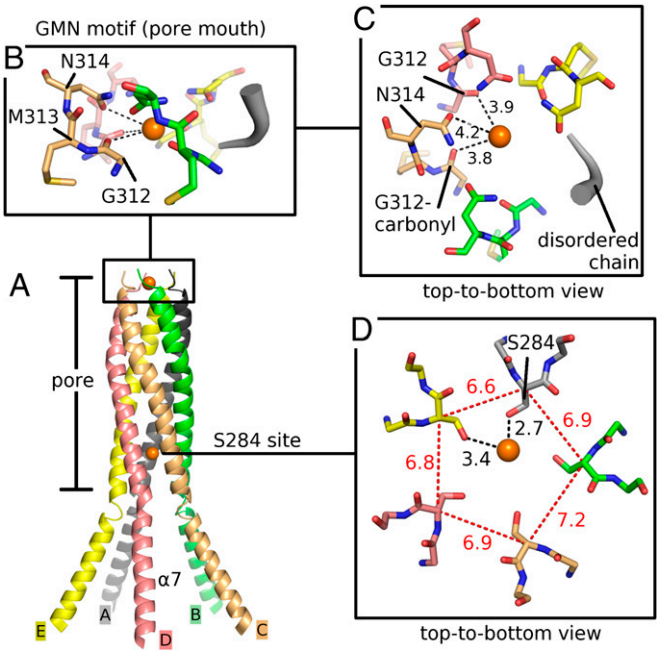

Fig. 2. Mg^{2+} sites inside the pore as observed in the X-ray structure of TmCorA-ΔNcc crystallized with Mg^{2+} present. (*A*) Five α7 helices (A to E) forming the CorA pore. Orange spheres indicate Mg^{2+} ions. (*B* and *C*) Close-up view of Mg^{2+} coordination at the GMN motif. Chain A is represented as a tube; a larger tube diameter indicates a higher B value. (*D*) Mg^{2+} coordination at the pore-lining residue S284 viewed along the pore axis. All distances in *C* and *D* are given in angstroms.

Results

Mutations That Disfavor the Closed State. Our inability to obtain crystals of TmCorA-WT in the absence of divalent ions might be caused by a higher degree of flexibility of the protein under these conditions. Without such a structure, however, it is difficult to characterize additional conformational states, which are necessary to explain the gating mechanism of the channel. To shift the protein toward an unlocked conformation, we instead aimed to loosen the coiled-coil interactions between helices α6 and α7 within the intracellular funnel domain (Fig. 1*A*), rationalizing that this region is likely to undergo structural changes in response to intracellular Mg^{2+} loss. In the closed TmCorA structures, R222 (α6) forms an intraprotomer salt bridge with E266 (α7), and K223 interacts with D263 of the neighboring protomer (Fig. S1*A*). In addition, we removed the N-terminal residues 1–25, which proved to be highly flexible in our proteolysis study independent of the Mg^{2+} concentration (see below); this truncation enhanced diffraction characteristics. Table S1 provides detailed statistics for the X-ray analysis of TmCorA-ΔNcc. The resulting ΔN25/R222A/K223A mutant will be called ΔNcc (N-truncated coiled-coil mutant). Like WT, ΔNcc adopts at least two different conformational states depending on the Mg^{2+} concentration (Fig. S1*B* for ΔNcc; see Fig. 5*A* for WT), as probed by limited proteolysis (19). However, TmCorA-ΔNcc shows a loss of function in our cellular complementation assay (Fig. S1*C*), possibly due to the inability of this channel to fully gate, because the coiled-coil mutation appears to stabilize a single or subset of conformations available to TmCorA-WT. Western blot analysis (Fig. S1*D*) shows that all of the mutants described here still associate with the cell membrane.

Identification of Mg^{2+} Ions and Asymmetry Within the Pore. In the presence of Mg^{2+} or Ca^{2+}, TmCorA-WT crystallizes in a fivefold-symmetric, closed conformation hosting 10 ions in the regulatory DCS (5 in M1, 5 in M2; Fig. 1*B*). When CorA was crystallized in the presence of 200 mM Ca^{2+}, an ion was unexpectedly observed right below the mouth of the pore (PDB ID code 2HN2), between G309 and G312 (19). Mg^{2+}, however, was only observed at the negatively charged D277 ring forming the pore exit (18) but could not be identified near the periplasmic region or any other pore section. Here, in the presence of Mg^{2+}, the crystal structure of TmCorA-ΔNcc reveals two Mg^{2+}-binding sites within the pore, one of them at the universally conserved GMN motif forming the periplasmic mouth of the pore (Fig. 2 *B* and *C*). The strong electron density (Fig. S2*A*) and refined distances of about 4 Å to carbonyl groups (G312) and asparagine side chains (N314) of the GMN motif are consistent with binding of a hydrated Mg^{2+} ion. Remarkably, only four of the five GMN motifs are well-ordered; the fifth N314 side chain appears to be disordered or flipped out, suggesting the selectivity filter in CorA may rearrange to accommodate the strict coordination of Mg^{2+} despite its pentameric architecture. A second Mg^{2+} ion is located in the intracellular pore section directly coordinated to one S284 hydroxyl side chain (Fig. 2*D* and Fig. S2*B*). This ion appears to also be in a water-mediated contact with at least one more adjacent serine side chain. A comparison of Cα-Cα distances located near the binding site shows that the two coordinating helices have moved slightly toward each other (by 0.2–0.6 Å), thereby breaking the fivefold symmetry of TmCorA observed in previous structures. Interestingly, this S284 coordination site aligns with a local minimum of an electrostatic energy profile of TmCorA-WT calculated along the pore axis (22). As seen in the

TmCorA-WT structures, in the presence of Mg^{2+} all 10 M1 and M2 sites are occupied by Mg^{2+}. Notably, the intracellular parts of the five ΔNcc protomers adopt different relative orientations to produce a slightly asymmetric conformation.

Increased Asymmetry of TmCorA-ΔNcc Without Mg^{2+}. We were also able to determine the X-ray structure of TmCorA-ΔNcc in the absence of divalent ions and found that only three M1 sites and one M2 site were occupied by monovalent Cs^+ ions (Fig. 3*A* and Movie S1). Empty sites correlate with increased distances between protomers (2–3 Å), which can be attributed to the repelling negative charges of the aspartate groups of the DCS. The unlocked protomers are seen to undergo three distinct motions (defined in Fig. 3*B*): lateral tilt (protomer A/C), radial tilt (protomer B/E), and *z* rotation (protomer D). Tilts and rotations range from 4° to 5°. The pronounced asymmetry of the divalent cation-free form of TmCorA-ΔNcc is already hinted at in the presence of Mg^{2+} but to a much lesser extent. Interestingly, Cs^+ is also binding to the GMN motif at an equivalent position. For ease of discussion, the five protomers have been given corresponding names (A through E) and color coding, allowing comparisons between the asymmetric motions of intracellular domains (Fig. 3*A*) with the asymmetric binding sites in the pore (Fig. 2).

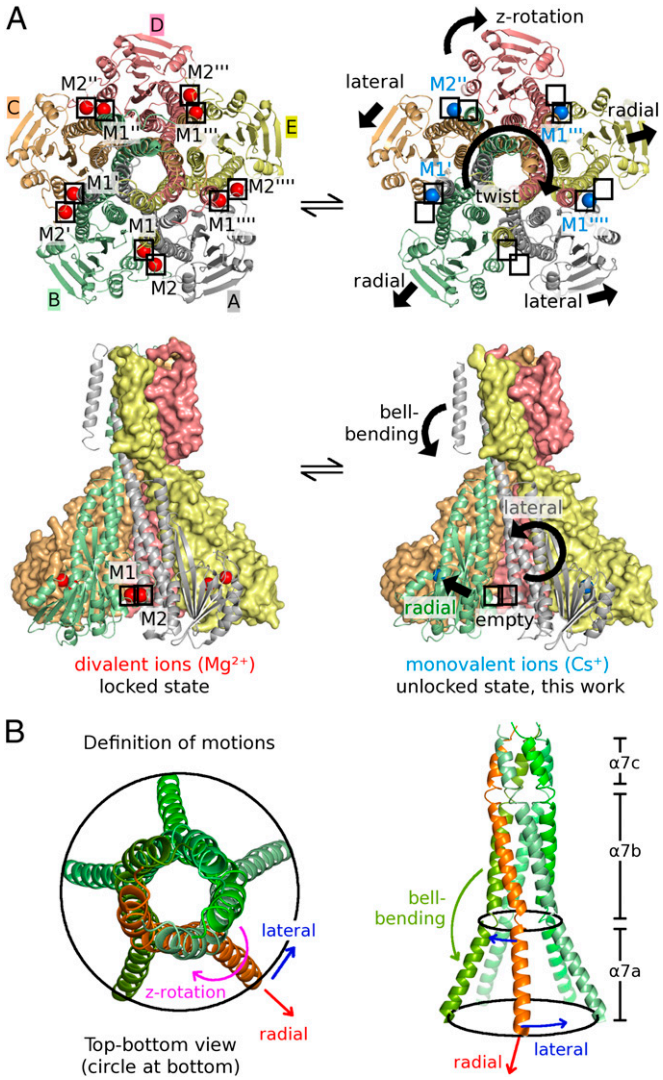

Fig. 3. (*A*) Effect of divalent ions on the CorA conformation. Representations on the left show the locked state of TmCorA-WT in the presence of Mg^{2+}, and those on the right show TmCorA-ΔNcc crystallized in the presence of Cs^+ instead of divalent ions. All motions were deduced from superpositions with the locked state. (*B*) Definition of motions: radial tilt (blue), lateral tilt (red), and *z* rotation (magenta). Only the five α7 helices are shown with these motions indicated for the orange helix. The bell bending (green) is related to an increased kink between α7a and α7b of a single helix.

The previous "closed" crystal structures show a very specific binding of divalent ions to the DCS. Divalent metals bind directly between aspartates D253 and D89′ at the protomer–protomer interface (M1; close-up in Fig. 1*A*), with a Mg^{2+}–O^- distance of 1.7–2.1 Å. None of the observed Cs^+ ions binds exactly like a divalent ion to M1. The distances between Cs^+ and protein residues of about 4 Å indicate weaker and water-mediated interactions. Superpositions confirm that asymmetry in the absence of divalent cations results mainly from rigid-body motions of the five cytosolic domains of protomers A to E, most likely permitted by the less specific interactions of monovalent ions (compared with Mg^{2+}) in the DCS. The pore radius of the unlocked structure, however, does not differ significantly from the locked WT conformations. Instead, the entire TM domain bends about 6° toward protomer B (bell-bending motion; Fig. 3*A*, *Lower Right*). The distance between TM2 (KKKKWL motif) and the intracellular α5-α6 loop (Fig. 1*A*) is shortest between protomers A and B. This bell-bending motion appears to pull away one single periplasmic loop (belonging to protomer A) from the pore mouth, thereby allowing ion coordination at the GMN motif (Fig. 2*C*). Whereas protomers A, C, D, and E remain largely unchanged compared with the previous "locked" structures of TmCorA-WT, in protomer B, the long α7 helix shows a significant bending with residue G274 of protomer B as the hinge for the bell-bending motion (Fig. S3).

MD Simulation on TmCorA-WT. In parallel to the determination of the unlocked structure by X-ray crystallography, two independent 700-ns MD simulations were carried out, respectively, with and without 10 regulatory Mg^{2+} ions in the DCS. As seen in Fig. 4, the absence of Mg^{2+} has a strong effect on the symmetry and dynamic fluctuations of the pentamer. Fig. 4*C* shows the distance, m1, between D253 and D89′ (regulatory site M1) during the simulation. In the presence of Mg^{2+}, m1 stays between 4 and 5 Å (left side of Fig. 4*C*), whereas without Mg^{2+}, it varies between 4 and 16 Å (right side of Fig. 4*C*). In the latter case, the changes are most pronounced for m1 and m1′′′′. The m1 distance (between protomers A and B) increases to almost 16 Å, whereas m1′′′′ (between protomers E and A), after an initial jump, stays below 6 Å. The smaller 6 Å distance of m1′′′′ is attributable to a neutralizing Na^+ ion trapped after 80 ns of simulation (Fig. 4*E*). Comparison with the ΔNcc-Cs^+ structure (Fig. 3*A*) shows a strikingly similar occupancy of M1 and M1′′′′ (protomers A, B, E). Accordingly, the protomers in the simulation were assigned names (A to E) identical to the ones chosen for the subunits in the two X-ray structures of TmCorA-ΔNcc (see Figs. 2 and 3). The remaining m1 distances undergo changes throughout the simulation, reflecting the capture and loss of monovalent ions in the various regulatory sites (Fig. S4*A*). A remarkable observation during the Mg^{2+}-free simulation is an increasing bell-bending motion during the first 250 ns (Fig. 4*F*), leading to a strongly bent state (Fig. 4*G*). The stalk helix α7′ (protomer B) displays the largest bending of 25° as is found in ΔNcc-Cs^+, where α7′ is also bent the most (Fig. S3). The bell-bending motion is accompanied by the formation of new salt bridges between adjacent protomers involving E201/E204 of the α5-α6 loop, the C-terminal KKKKWL motif, and the conserved residue K292 (Fig. 4 *A*, *B*, and *D*). These interactions happen only on one side of the pentamer, mainly between protomers A (colored gray) and B (green). The drastic increase of the bell-bending after 150 ns coincides with an increased tilt of the pore axis against the membrane normal and a formation of additional salt bridges between the intracellular CorA surface and the lipid bilayer (Fig. S5). The pore is hydrated for about 25 ns in the presence of Mg^{2+} but subsequently reverts to the dehydrated

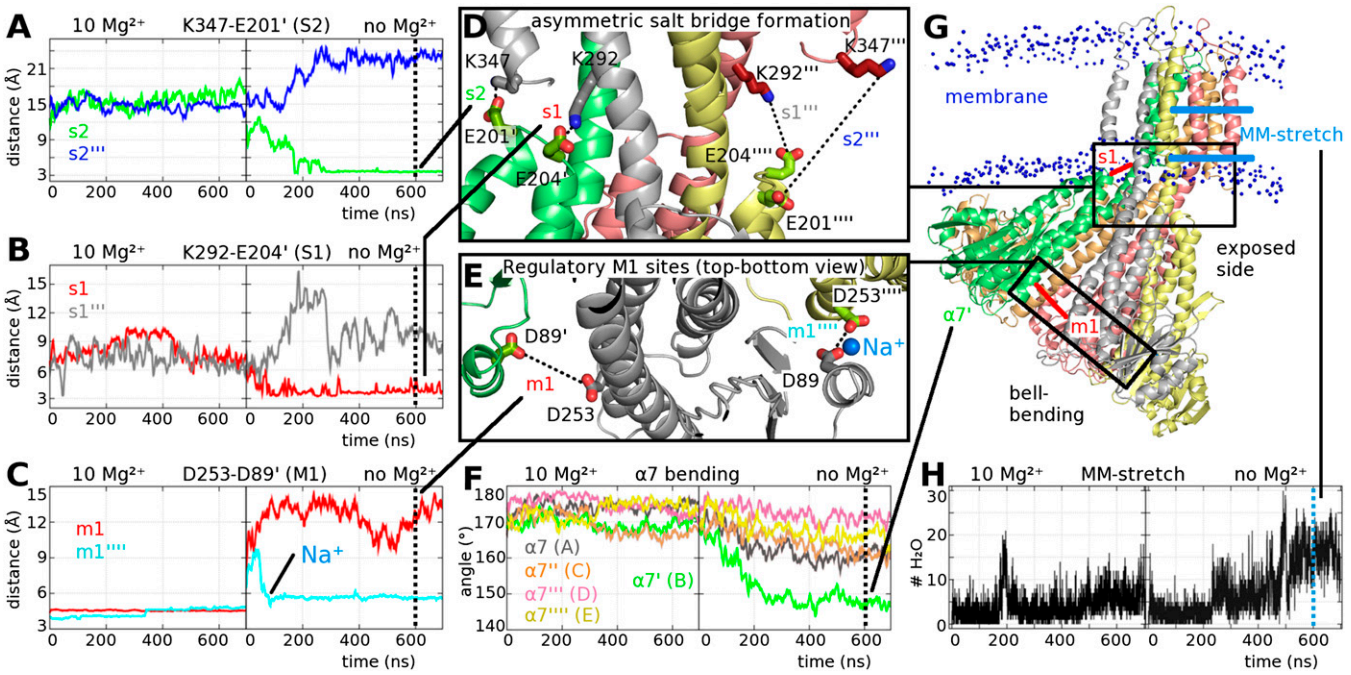

Fig. 4. Analysis of structural fluctuations from 700-ns MD simulations of TmCorA-WT with and without Mg^{2+} ions present. Both simulations include Na^+ for electroneutrality. Graphs *A*–*C* show only two of five distances for clarity. For the full set of distances, see Fig. S4. (*A*) Distance between K347 (Nζ) and E201′ (Cδ). (*B*) Distance between K292 (Nζ) and E204′ (Cδ). In *A* and *B*, a distance close to 3 Å indicates a salt bridge. (*C*) Distance between D253 (Cγ) and D89′ (Cγ). A distance between 4 and 6 Å indicates the presence of a neutralizing cation. (*D*) Close-up view of the formation of salt bridges monitored in *A* and *B*. (*E*) Close-up view of distances m1 and m1′′′′ monitored in *C*. (*F*) Angle between V248, L280, and I310 (all Cα). The graph is color coded to match the protomer representation in *G*. (*G*) Snapshot of the CorA pentamer and membrane after 600 ns of simulation. The phosphorus atoms of the 1,2-dimyristoyl-*sn*-glycero-3-phosphocholine (DMPC) bilayer are shown as blue spheres. (*H*) Water count in the MM stretch (constricted hydrophobic pore area from M302 to M291).

state. In contrast, without Mg^{2+} the pore becomes gradually hydrated and reaches a permanent hydration in the last 180 ns of the simulation (Fig. 4*H*).

Comparing the changes in the crystal structures with those achieved in the simulations, we find that the individual protomers undergo similar rigid-body motions with a similar magnitude between 50 and 150 ns. After 150 ns, these motions become more pronounced in the simulation, presumably because of protein–bilayer interactions. In either case, the pentamer transforms from a symmetric Mg^{2+}-locked state to an asymmetric Mg^{2+}-free state with a strong bend between the cytosolic and transmembrane domains.

Probing Mg^{2+}-Dependent Conformational Changes in Solution. Protease-susceptibility assays also support two different conformational states of CorA. At Mg^{2+} concentrations higher than 0.5 mM, the channel protein is much more resistant against proteolysis (19). Fig. 5*A* shows trypsin digestion of TmCorA-WT as a function of Mg^{2+} concentration with the major cleavage products identified by liquid chromatography–tandem mass spectrometry (LC MS/MS) and N-terminal Edman sequencing. In the presence of trypsin, a band appears below the 26-kDa marker, and its intensity decreases when the Mg^{2+} concentration increases. The corresponding cleavage site is at R202 and K205 in the α5-α6 loop (Fig. 5*C*), which forms a ring around the pore slightly below the main hydrophobic constriction. At low Mg^{2+} levels, the majority of the protein is cleaved at this position, whereas at concentrations higher than 0.5 mM, most of the protein is protected. Monovalent ions (Li^+, Na^+, K^+, Rb^+, Cs^+) are not able to provide this protection (19). Notably, this cleavage site is located in the area that becomes exposed during bell-bending (Fig. 4*G*). The Mg^{2+} dependence of this site can be abolished by replacing regulatory site M1 with a permanent salt bridge as in the mutant D253K (Fig. S6*A*). Trypsin cleavage is also almost fully abrogated in mutant R202G, confirming the mass spectrometric assignment (Fig. S6*B*). A weak band that is already present in freshly prepared samples was identified as the intracellular domain cleaved at conserved residue K292, which is part of the basic sphincter (positioned at the membrane–aqueous interface at the level of the most constricted pore section) and takes part in a salt-bridge with the α5-α6 loop, also observed in the MD study (s1 in Fig. 4*D*). In the same study, K292 and R202 become both widely exposed and more mobile during bell-bending, linking computational, structural, and biochemical results in support of a connection between this conformation and low intracellular Mg^{2+} levels. The majority of TmCorA-WT is cleaved either at K9 or K22 (Fig. 5*B*) in the presence of trypsin. This represents the cleavage of the N terminal lid removed in the ΔNcc construct, which covers the DCS in the closed state (Fig. 5*D*) and appears to be rather flexible regardless of Mg^{2+} concentration, consistent with the improved diffraction characteristics of the mutant. Exposing three unrelated proteins to identical proteolysis conditions showed that the observed increased protection of TmCorA-WT and TmCorA-ΔNcc from proteolytic attack is not due to inhibition of trypsin (Fig. S7).

Discussion

Nonconcerted Allosteric Regulation of CorA. In this study, both crystallography and MD simulation expose a severe asymmetry in TmCorA caused by removal of Mg^{2+}. Pronounced asymmetry has also been observed in the putatively inactivated form of a bacterial voltage-gated sodium (Na^+) channel (26, 27) and the Na^+-selective form of an acid-sensing ion channel (28). The observation that only half of the regulatory sites are occupied in the presence of monovalent ions in TmCorA-ΔNcc (Fig. 3*A* and Fig. S4*A*) may be analogous to the heteropentameric acetylcholine (ACh) receptor (29), where only two ACh molecules bind to opposing sites of the five possible protomer interfaces. In TmCorA, we found that

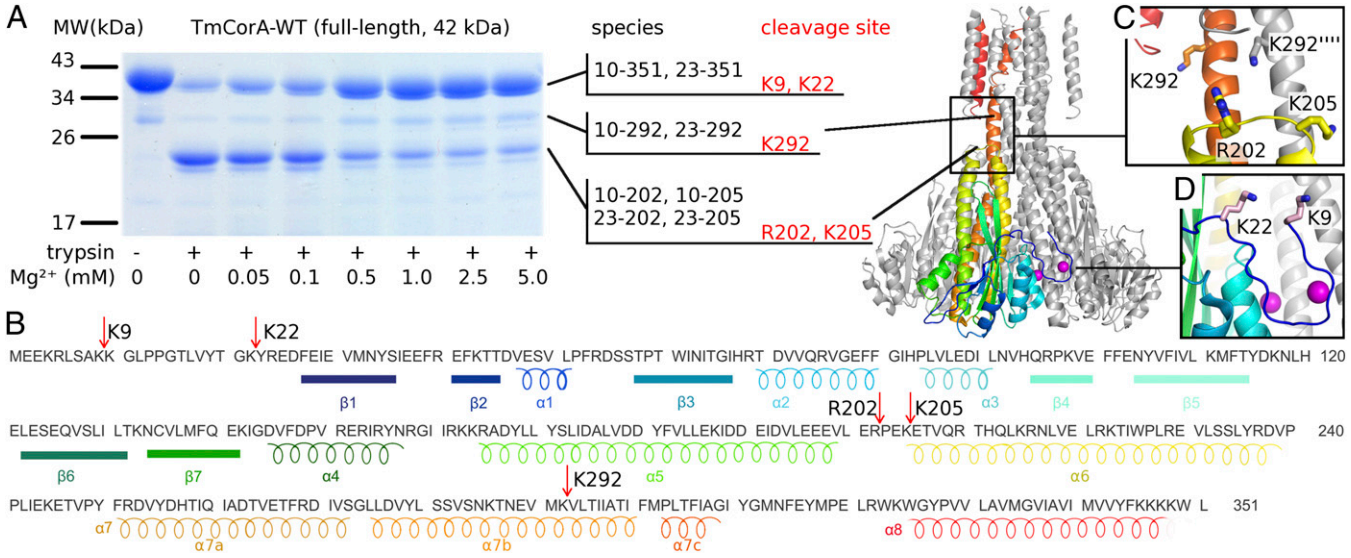

Fig. 5. Influence of Mg^{2+} concentration on trypsin digestion. (*A*) SDS/PAGE analysis with identified species and cleavage sites shown for each susceptible site. (*B*) Sequence of TmCorA with cleavage sites is indicated by red arrows. Structural elements are color-coded matching the protein model representation in *A*. (*C*) Close-up view of the cleavage sites at R202/K205 and K292. (*D*) Close-up view of the N-terminal cleavage sites K9 and K22.

monovalent ions are not able to lock the pentamer in the closed state like Mg^{2+}, which connects aspartate residues of adjacent protomers by direct COO^{-}–Mg^{2+}–COO^{-} coordination. The negatively charged α5-α6 loop faces the basic sphincter but in the closed conformation, these two regions do not come close enough to form salt bridges (Fig. 6, *Left*). By contrast, at low intracellular Mg^{2+} concentrations, a combination of lateral and radial tilting of two adjacent protomers allows salt bridges between amino acids in the α5-α6 loop and K292 on one side of the CorA pentamer, changing the tilt of pore forming helix α7. (Fig. 6, *Right*). These electrostatic interactions are part of the observed bell-bending motion and might initiate Mg^{2+} influx by pulling away a single chain (belonging to protomer A; gray) from the pore mouth (Fig. 2*C*). Additionally, the positive side chains of the basic sphincter closest to the most constricted pore region become neutralized, lowering the electrostatic barrier for Mg^{2+} influx. In the simulation without Mg^{2+}, the other four α5-α6 loops of the CorA pentamer become more mobile and exposed (Fig. S4*B* and Fig. 4*G*), consistent with our finding of increased trypsin susceptibility at Mg^{2+} concentrations below 0.5 mM (Fig. 5).

Selectivity Filter. Ion selectivity has remained a mystery in CorA. In the well-studied tetrameric potassium (K^{+}) channels, a set of mostly dehydrated K^{+} ions is stabilized along the trajectory of a fourfold symmetric pore by carbonyl groups mimicking the geometry of the ions' hydration shells (30). Mg^{2+} selectivity in the CorA filter must rely on a completely different principle. Removal of all hydrating water molecules is energetically much more costly for Mg^{2+} than for K^{+} (31) and could not easily be compensated by the fivefold symmetry of CorA. The observed binding of a hydrated Mg^{2+} (this work; Fig. 2) provides direct evidence that the universally conserved and essential GMN motif is critically involved in CorA selectivity. Details of how Mg^{2+} is selected over other ions, and why Co^{2+} and Ni^{2+} are also transported substrates (4) remain unknown. Mg^{2+}, Co^{2+}, and Ni^{2+} share relatively slow water exchange rates of ~10^{5} water molecules per second (32) and preferably form hexahydrated water complexes very similar in geometry and size (25, 33). Although other ions such as Na^{+}, K^{+}, Cs^{+}, and Ca^{2+} can also form octahedral aquo complexes, their diameters are larger and this is not their most distinct coordination geometry (34); these ions also have much higher water exchange rates (~10^{9} water molecules second). The periplasmic mouth of the CorA pore seems to recognize the octahedral geometry of $[Mg(H_2O)_6]^{2+}$, selecting it over other ions (Ca^{2+}, Na^{+}, K^{+}) probably because of its shape and higher stability. Preliminary electrophysiological experiments on CorA (16) indicate a very high influx rate (>10^{7} ions/second), suggesting transport of Mg^{2+} with its entire first hydration shell intact or facilitation of an at most partial dehydration by the formation of stabilizing interactions with CorA. $[Co(NH_3)_6]^{3+}$, which is not transported by CorA (23) or its homolog Mrs2 (15) but strongly inhibits Mg^{2+} influx, provides additional support for such a scenario. In the proposed conductive conformation, the Mg^{2+}-bound selectivity filter of CorA does not follow the example of K^{+} channels, the filters of which are assumed to remain largely symmetric during ion conduction but aligns with the asymmetric selectivity filter of the voltage-gated Na^{+} channel (35) and the asymmetric conformation of the Na^{+}-conductive acid-sensing ion channel (28). The second Mg^{2+}-binding site in the pore of TmCorA-ΔNcc at S284 (Fig. 2*D*) further shows that a partially

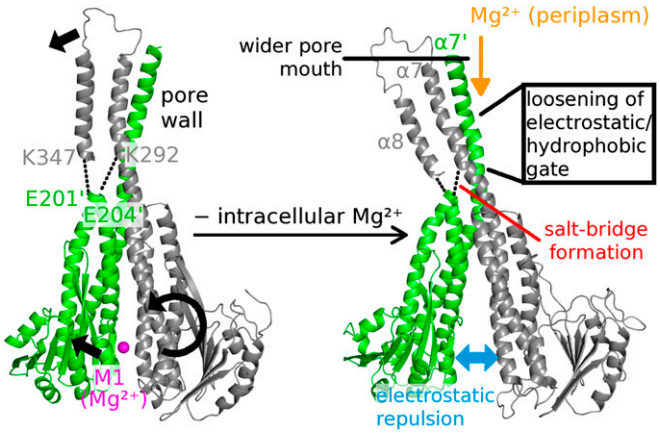

Fig. 6. Model of the allosteric regulation of Mg^{2+} influx. The regulating Mg^{2+} ion is shown in pink, and the orange arrow indicates the direction of transport. Black arrows indicate the movements of the two adjacent protomers (shown in gray and green) in response to the loss of the regulatory divalent ion. The model is based on the results of both X-ray structures and MD simulations.

dehydrated Mg^{2+} ion can be stabilized in the pore and suggests that Mg^{2+} is not moving on a symmetric pore axis but rather along the wall of an asymmetric pore, again reminiscent of recent computational results on the Na^{+} channel (36, 37). Our present and previous (22) MD simulations suggest that the hydrophobic stretches of the CorA pore are much more likely to become occupied by water molecules at low intracellular Mg^{2+} levels, consistent with the permeation of hydrated Mg^{2+} ions.

Conclusions

Our study does not provide evidence for a concerted movement of the five protomers forming the CorA channel; in contrast, it reveals a striking asymmetry involved in allosteric regulation and ion stabilization in the pore. Sequential rigid-body motions allow the formation of salt bridges that influence the tilts of individual pore-forming helices. The observation of a hydrated Mg^{2+} ion at the mouth of the pore suggests that the universally conserved GMN motif is only accessible in the asymmetric state of the channel and that it is indeed the selectivity filter of the CorA-Mrs2-Alr1 superfamily. In contrast to K^{+} channels, it seems Mg^{2+} ions with their first hydration shell intact are selected over other ions by CorA, and at least part of this hydration shell is required for transport across the membrane. The concepts illuminated in our study allow fast regulation of Mg^{2+} concentration in biological systems, and they also conform with this ion's unique chemistry and biological relevance.

Methods

To test for competency in Mg^{2+} transport, expression plasmids for WT and mutant TmCorA were transformed into *Escherichia coli* strain BW25113 as published (38). Figures of proteins were generated with PYMOL (DeLano Scientific). For further details, see *SI Methods*.

ACKNOWLEDGMENTS. We thank Pawel Grochulski and the staff members of the Canadian Macromolecular Crystallography Facility for assistance with crystallographic data collection; Osamu Nureki (Tokyo, Japan) for providing Mg^{2+} auxotrophic strain BW25113; and the Shared Hierarchical Academic Research Computing Network (SHARCNET) (Canada) for generous allocations of computing resources. Part of the research described in this paper was performed at the Canadian Light Source, which is supported by the Natural Sciences and Engineering Research Council of Canada, the National Research Council Canada, the Canadian Institutes of Health Research, the Province of Saskatchewan, Western Economic Diversification Canada, and the University of Saskatchewan. E.F.P. and R. Pomès received support from Canadian Institutes of Health Research (CIHR) Grants MOP-86548 and MOP-43949, respectively, and the Canada Research Chairs Program. This research was funded in part by the Ontario Ministry of Health and Long Term Care.

1. Cowan JA (2002) Structural and catalytic chemistry of magnesium-dependent enzymes. *Biometals* 15(3):225–235.
2. Brunet S, Scheuer T, Klevit R, Catterall WA (2005) Modulation of CaV1.2 channels by Mg2+ acting at an EF-hand motif in the COOH-terminal domain. *J Gen Physiol* 126(4): 311–323.
3. Li FY, et al. (2011) Second messenger role for Mg2+ revealed by human T-cell immunodeficiency. *Nature* 475(7357):471–476.
4. Kehres DG, Maguire ME (2002) Structure, properties and regulation of magnesium transport proteins. *Biometals* 15(3):261–270.
5. Kersey CM, Agyemang PA, Dumenyo CK (2012) CorA, the magnesium/nickel/cobalt transporter, affects virulence and extracellular enzyme production in the soft rot pathogen Pectobacterium carotovorum. *Mol Plant Pathol* 13(1):58–71.
6. Bui DM, Gregan J, Jarosch E, Ragnini A, Schweyen RJ (1999) The bacterial magnesium transporter CorA can functionally substitute for its putative homologue Mrs2p in the yeast inner mitochondrial membrane. *J Biol Chem* 274(29):20438–20443.
7. Zsurka G, Gregán J, Schweyen RJ (2001) The human mitochondrial Mrs2 protein functionally substitutes for its yeast homologue, a candidate magnesium transporter. *Genomics* 72(2):158–168.
8. Liu GJ, Martin DK, Gardner RC, Ryan PR (2002) Large Mg(2+)-dependent currents are associated with the increased expression of ALR1 in Saccharomyces cerevisiae. *FEMS Microbiol Lett* 213(2):231–237.
9. Li L, Tutone AF, Drummond RSM, Gardner RC, Luan S (2001) A novel family of magnesium transport genes in Arabidopsis. *Plant Cell* 13(12):2761–2775.
10. Kolisek M, et al. (2003) Mrs2p is an essential component of the major electrophoretic Mg2+ influx system in mitochondria. *EMBO J* 22(6):1235–1244.
11. Piskacek M, Zotova L, Zsurka G, Schweyen RJ (2009) Conditional knockdown of hMRS2 results in loss of mitochondrial Mg(2+) uptake and cell death. *J Cell Mol Med* 13(4): 693–700.
12. Assou S, et al. (2009) A gene expression signature shared by human mature oocytes and embryonic stem cells. *BMC Genomics* 10:10.
13. Chen Y, et al. (2009) Human mitochondrial Mrs2 protein promotes multidrug resistance in gastric cancer cells by regulating p27, cyclin D1 expression and cytochrome C release. *Cancer Biol Ther* 8(7):607–614.
14. Wolf FI, Trapani V (2009) Multidrug resistance phenotypes and MRS2 mitochondrial magnesium channel: Two players from one stemness? *Cancer Biol Ther* 8(7):615–617.
15. Schindl R, Weghuber J, Romanin C, Schweyen RJ (2007) Mrs2p forms a high conductance Mg2+ selective channel in mitochondria. *Biophys J* 93(11):3872–3883.
16. Moomaw AS, Maguire ME (2010) Cation selectivity by the CorA Mg2+ channel requires a fully hydrated cation. *Biochemistry* 49(29):5998–6008.
17. Lunin VV, et al. (2006) Crystal structure of the CorA Mg2+ transporter. *Nature* 440 (7085):833–837.
18. Eshaghi S, et al. (2006) Crystal structure of a divalent metal ion transporter CorA at 2.9 angstrom resolution. *Science* 313(5785):354–357.
19. Payandeh J, Pai EF (2006) A structural basis for Mg2+ homeostasis and the CorA translocation cycle. *EMBO J* 25(16):3762–3773.
20. Knoop V, Groth-Malonek M, Gebert M, Eifler K, Weyand K (2005) Transport of magnesium and other divalent cations: Evolution of the 2-TM-GxN proteins in the MIT superfamily. *Mol Genet Genomics* 274(3):205–216.
21. Payandeh J, et al. (2008) Probing structure-function relationships and gating mechanisms in the CorA Mg2+ transport system. *J Biol Chem* 283(17):11721–11733.
22. Chakrabarti N, Neale C, Payandeh J, Pai EF, Pomès R (2010) An iris-like mechanism of pore dilation in the CorA magnesium transport system. *Biophys J* 98(5):784–792.
23. Kucharski LM, Lubbe WJ, Maguire ME (2000) Cation hexaammines are selective and potent inhibitors of the CorA magnesium transport system. *J Biol Chem* 275(22): 16767–16773.
24. Hu J, Sharma M, Qin H, Gao FP, Cross TA (2009) Ligand binding in the conserved interhelical loop of CorA, a magnesium transporter from Mycobacterium tuberculosis. *J Biol Chem* 284(23):15619–15628.
25. Markham GD, Glusker JP, Bock CW (2002) The arrangement of first- and second-sphere water molecules in divalent magnesium complexes. *J Phys Chem B* 106(19): 5118–5134.
26. Payandeh J, Gamal El-Din TM, Scheuer T, Zheng N, Catterall WA (2012) Crystal structure of a voltage-gated sodium channel in two potentially inactivated states. *Nature* 486(7401):135–139.
27. Zhang X, et al. (2012) Crystal structure of an orthologue of the NaChBac voltage-gated sodium channel. *Nature* 486(7401):130–134.
28. Baconguis I, Gouaux E (2012) Structural plasticity and dynamic selectivity of acid-sensing ion channel-spider toxin complexes. *Nature* 489(7416):400–405.
29. Unwin N (2005) Refined structure of the nicotinic acetylcholine receptor at 4A resolution. *J Mol Biol* 346(4):967–989.
30. Doyle DA, et al. (1998) The structure of the potassium channel: Molecular basis of K+ conduction and selectivity. *Science* 280(5360):69–77.
31. Draper DE (2004) A guide to ions and RNA structure. *RNA* 10(3):335–343.
32. Helm L, Mehrbach AE (1999) Water exchange on metal ions: Experiments and simulations. *Coord Chem Rev* 187(1):151–181.
33. Cotton FA, Daniels LM, Murillo CA, Quesada JF (1993) Hexaaqua dipositive ions of the first transition series: New and accurate structures; expected and unexpected trends. *Inorg Chem* 32(22):4861–4867.
34. Ohtaki H, Radnai T (1993) Structure and dynamics of hydrated ions. *Chem Rev* 93(3): 1157–1204.
35. Payandeh J, Scheuer T, Zheng N, Catterall WA (2011) The crystal structure of a voltage-gated sodium channel. *Nature* 475(7356):353–358.
36. Corry B, Thomas M (2012) Mechanism of ion permeation and selectivity in a voltage gated sodium channel. *J Am Chem Soc* 134(3):1840–1846.
37. Furini S, Domene C (2012) On conduction in a bacterial sodium channel. *PLOS Comput Biol* 8(4):e1002476.
38. Hattori M, et al. (2009) Mg(2+)-dependent gating of bacterial MgtE channel underlies Mg(2+) homeostasis. *EMBO J* 28(22):3602–3612.